This is the accepted manuscript of the article that appeared in final form in **Composite Structures** 190 : 169-178 (2018), which has been published in final form at https://doi.org/10.1016/j.compstruct.2018.02.021. © 2018 Elsevier under CC BY-NC-ND license (http://creativecommons.org/licenses/by-nc-nd/4.0/)

ANALYSIS OF DCB TEST OF ANGLE-PLY LAMINATES INCLUDING BENDING-TWISTING COUPLING

J. De Gracia[a,*], A. Boyano[a], A. Arrese[b], F. Mujika[b]

Materials+Technologies Group/Mechanics of Materials

[a] Department of Mechanical Engineering, Faculty of Engineering of Vitoria-Gasteiz, University of the Basque Country (UPV/EHU), Nieves Cano, 12, 01006 Vitoria-Gasteiz, Spain

[b] Department of Mechanical Engineering, Faculty of Engineering of Gipuzkoa, University of the Basque Country (UPV/EHU), Plaza de Europa, 1, 20018 San Sebastián, Spain

*Corresponding author. E-mail: juan.degracia@ehu.eus

Abstract

Interlaminar fracture of angle-ply symmetric and anti-symmetric laminates by means of the Double Cantilever Beam test has been analyzed. As the cracked arms are symmetric in both cases, bending-twisting coupling occurs. Nevertheless, the effect of that coupling is different in symmetric and anti-symmetric cases. In symmetric cases, it induces a non-uniform aperture of the arms associated to mode I. In anti-symmetric cases, the effect is a sliding of both arms associated to mode III. The analytic approach of the energy release rate includes those coupling effects. Besides the present approach, experimental results are reduced with a previous approach that does not include coupling effects and with the area method.

Keywords: Delamination; Double Cantilever Beam; Multidirectional, coupling effects

1. Introduction

One of the most common damage mechanism in laminated composites is delamination, due to the low interlaminar strength of these materials. According to linear elastic fracture mechanics (LEFM) there are three modes of fracture, mode I or opening mode, mode II or sliding mode and mode III or tearing mode [1].

The Double Cantilever Beam (DCB) test is widely used for the determination of interlaminar fracture toughness in mode I. The LEFM principles are applied and used to measure the energy dissipated per unit area of crack growth, known as the energy release rate G_I, of unidirectional laminates. The test has been standardized for carbon fiber reinforced plastic (CFRP) specimens [2, 3]. Despite the fact that the test is very simple, it requires the optical determination of the growing interlaminar crack. Nevertheless, sometimes the crack tip is difficult to observe and it can prevent from obtaining a good characterization of the material. Some authors have dealt with this issue by means of different methods. Szekrényes uses a transparent material in order to identify the crack front [4]. Yoshihara and Kawamura [5] obtained compliance independently from the crack length using the longitudinal strain of the top surface of the specimen. De Moura et al. [6] proposed a method, based on a crack equivalent concept, to consider the fracture process zone at the crack tip. De Gracia et al. [7] proposed a method to determine the crack length by means of the change on the specimen compliance during the test.

In spite of standards have been developed for DCB unidirectional specimens, this test configuration has been also used to calculate G_{Ic} of multidirectional laminates [8, 9, 10]. Choi et al. [11] and Morais [12] have assessed the applicability of the test for those laminates, determining that it can be valid if deviations of the delamination from the central plane are avoided. Factors which may affect seriously the test in the case of

multidirectional specimens are laminate lay-up, symmetry of the laminate, curved crack front, mode mixture, residual stresses or damage during the crack growth (fiber bridging effect, fiber matrix debonding, or fiber breakage) [13]. An appropriate selection of the stacking sequence may prevent those issues, making their effect on G_{Ic} negligible and leading to a nearly pure mode I [14]. Nevertheless, this is not always possible since the industry uses laminates with a wide range of sequences and therefore couplings and residual stresses are often present. Taking all these factors into account, in addition to the fact that initiation value is the most conservative toughness value, delamination toughness from the DCB test on multidirectional laminates should probably be quantified just for initiation values.

Extensive research concerning mode I has been led to develop analytical solutions for DCB specimens. The elastic foundation was first applied by Kanninen [15] for the DCB specimen to model the deflection and rotation at the crack tip zone improving the application of the simple beam theory. Williams [16] extended Kanninen's model for orthotropic materials, while Ozdil and Carlsson [17] extended it to angle-ply laminates taking into account out-of-plane stiffness. Szekrényes [18] presented an improved analysis including Winkler–Pasternak foundation, transverse shear, Saint–Venant effect and crack tip shear deformation. Olsson [19] reviewed these and posterior works [20, 17, 21] concerning beams on elastic foundation, concluding that the use of energy approaches to incorporate the crack tip compliance or Timoshenko beams on a Winkler foundation are the methods that best fit to FEM results. Other methods to obtain an analytical solution involve beam theory and the specimen compliance [7] or include a rotational spring to a clamped beam [22, 23].

The previous models regarding interlaminar toughness in multidirectional laminates are mainly applied to stacking sequences that avoid bending-twisting coupling. However,

twisting curvatures and residual stresses due to hygrothermal effects can appear when other sequences are used. Concerning these effects, a new analytical approach has been recently proposed [24]. The model presented leads to calculate the total energy release rate in the DCB test including the contribution residual stresses to the energy release rate. In the mentioned work, the semi-laminates or cracked arms of the specimen were anti-symmetric and thus there was not bending-twisting coupling in each arm. Moreover, as a first approach, the distribution of the twisting moment per unit length across the width was assumed to be uniform.

The main goal of the present study is to include the effect of the bending-twisting coupling in the analysis of the DCB test, in order to complete the study mentioned previously [24]. The sequences studied are $\left[\left(\pm 45/\pm 45\right)_s\right]_s$ symmetric and $\left[\left(\pm 45/\pm 45\right)_s\right]_{as}$ anti-symmetric. The properties of the symmetric cracked arms are the same in both cases, but the orientation of the plies that form the interlaminar crack is different, $\left(+45/+45\right)$ in the first case and $(+45/-45)$ in the second one.

As the arms of the specimens studied are symmetric, the existence of bending-twisting coupling provokes a rotation in each cracked arm induced by the bending moment applied by means of piano hinges or load blocks. In the case of anti-symmetric laminates both arms rotate in the same sense, whereas if the laminate is symmetric the rotations are opposite, as shown in Fig. 1. Then, there is a rigid body rotation of the non-cracked part in the case of anti-symmetric specimens. In the case of symmetric laminates there is a non-uniform load distribution applied to the piano hinges, whose resultant and resultant moment are the applied force P and an unknown twisting moment m_t, respectively, preventing the rigid body rotation of the non-cracked part.

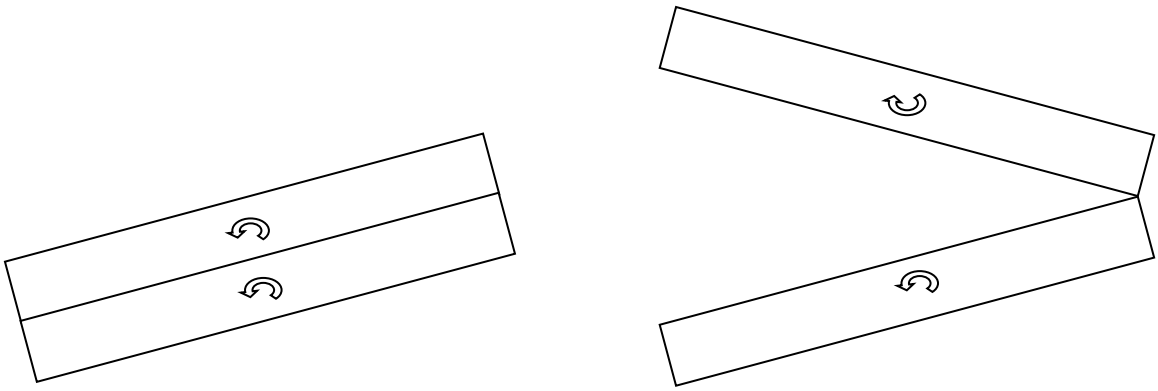

Fig. 1 Rotations at the crack tip. a) Anti-symmetric laminate b) Symmetric laminate

Besides the analysis of the contribution to the energy, the analytic approach has been modified with respect to [24] in order to take into account that the distribution of the twisting moment per unit length across the width is not uniform.

Nomenclature

a	Delamination length (*mm*)
$[a],[b],[c]$	Compliance matrices
a_{mn}	In-plane compliance coefficients (*mm/N*)
b	DCB specimen width (*mm*)
d_{mn}	Flexural compliance coefficients $(N \cdot mm)^{-1}$
$\{e\}_k$	Hygrothermal strains matrix at lamina k
F_1, F_2, F_3	Equivalent point forces for distributed load (*N*)
G_I, G_{II}, G_{III}	Strain energy release rate in mode I, II, III (J/m^2)
G_C	Critical strain energy release rate (J/m^2)
h	Thickness of the cracked arm (*mm*)
L	Length of the specimen (*mm*)

$\{\bar{M}\}$	Matrix of the sum of mechanical and hygrothermal moments
M_i	Bending moment per unit length at section i (N)
M_{s_i}	Twisting moment per unit length at section i (N)
m_i	Bending moment at section i ($N{\cdot}mm$)
m_{t_i}	Twisting moment at section i ($N{\cdot}mm$)
$\{\bar{N}\}$	Matrix of the sum of mechanical and hygrothermal forces
N_x^{HT}, N_y^{HT}	Hygrothermal forces per unit length (N/mm)
P	Opening load on the DCB specimen (N)
$[Q]_k$	Reduced stiffness matrix at lamina k
q_{10}, q_{30}	Maximum intensities of the distributed forces in the model (N/m)
S_{ij}	Compliance coefficients of lamina k
U^*	Complementary strain energy (N/m)
u, v, w	Displacement components
u_0, v_0, w_0	Displacement components in the middle plane
V_q, V_r	Out-of-plane shear stress resultants
x_1, x_2, x_3	Parameters of the distributed forces (mm)
z_k	Distance from the mid-plane to the lower surface of the k^{th} layer.
$\alpha_0, \alpha_1, \alpha$	Parameters depending on x_1, x_2, x_3
$\gamma_{xy} = \gamma_s$	In-plane shear strain
$\gamma_{yz} = \gamma_q, \gamma_{zx} = \gamma_r$	Out-of-plane shear strains
δ_i	Generalized displacement at point i in the direction of F_i

$\varepsilon_x, \varepsilon_y, \varepsilon_z$	Normal strains
$\varepsilon_x^0, \varepsilon_y^0$	Normal strains in the middle surface
θ_x	Bending angle
θ_y	Twisting angle
κ_x, κ_y	Bending curvatures of the middle surface
κ_s	Twisting curvature of the middle surface
$\{\sigma\}_k$	In plane stresses matrix at lamina k

2. Analytical approach

2.1. Displacement and strain fields

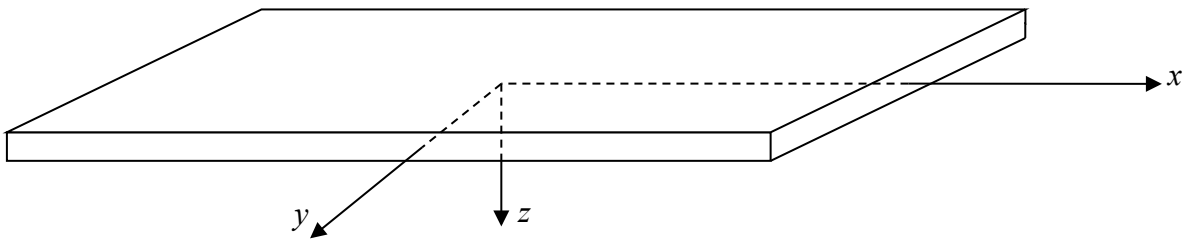

Fig. 2 Reference system adopted

In order to model the specimens used in this work strip geometry is assumed. Fig. 2 shows the reference system used in the present analysis. The displacement field is assumed to be given by:

$$\begin{aligned} u &= u_0(x,y) + z\theta_x(x,y) \\ v &= v_0(x,y) + z\theta_y(x) \\ w &= w_0(x,y) = w_0(x) - y\theta_y(x) \end{aligned} \tag{1}$$

Where u and v are in-plane displacements in x and y directions respectively and w is

the normal deflection. u_0, v_0 and w_0 are the displacements along the coordinate lines of a point in the xy plane ($z=0$), θ_x is the bending angle and θ_y is the twisting angle. This displacement field takes into account bending and twisting. Strains associated to this field can be found from Eq.(1), resulting in:

$$\begin{aligned}
&\varepsilon_x = u_{,x} = \varepsilon_x^0 + z\kappa_x \\
&\varepsilon_y = v_{,y} = \varepsilon_y^0 + z\kappa_y \\
&\varepsilon_z = 0 \\
&\gamma_{xy} = \gamma_s = u_{,y} + v_{,x} = \gamma_{xy}^0 + z\kappa_{xy} \\
&\gamma_{xz} = u_{,z} + w_{,x} = \theta_x + w_{0,x} - y\theta_y' \\
&\gamma_{yz} = v_{,z} + w_{,y} = \theta_y - \theta_y = 0
\end{aligned} \tag{2}$$

In Eq. (2) the strains and curvatures of the middle surface of the laminate are, respectively:

$$\begin{aligned}
&\varepsilon_x^0 = u_{0,x};\ \varepsilon_y^0 = v_{0,y};\ \gamma_s^0 = u_{0,y} + v_{0,x} \\
&\kappa_x = \theta_{x,x};\ \kappa_y = \theta_{y,y} = 0;\ \kappa_{xy} = \kappa_s = \theta_{x,y} + \theta_{y,x} = \theta_{x,y} + \theta_y'
\end{aligned} \tag{3}$$

2.2. Stress strain relations

2.2.1. In-plane relation

In-plane and out-of-plane behavior are not coupled and can be analyzed separately. The stress strain relations for in-plane components are:

$$\begin{Bmatrix} \sigma_x \\ \sigma_y \\ \tau_s \end{Bmatrix}_k = \begin{bmatrix} Q_{xx} & Q_{xy} & Q_{xs} \\ Q_{xy} & Q_{yy} & Q_{ys} \\ Q_{xs} & Q_{ys} & Q_{ss} \end{bmatrix}_k \left(\begin{Bmatrix} \varepsilon_x \\ \varepsilon_y \\ \gamma_s \end{Bmatrix} - \begin{Bmatrix} e_x \\ e_y \\ e_s \end{Bmatrix}_k \right) \tag{4}$$

In abbreviated form:

$$\{\sigma\}_k = [Q]_k \left(\{\varepsilon\} - \{e\}_k \right) = [Q]_k \left(\{\varepsilon^0\} + z\{\kappa\} - \{e\}_k \right) \tag{5}$$

Where $\{\sigma\}_k$ are in-plane stresses at lamina k, $[Q]_k$ are the reduced stiffness coefficients at lamina k, $\{\varepsilon^0\}$ are in-plane strains of the reference plane; $\{\kappa\}$ the curvatures and

$\{e\}_k$ the hygrothermal strains given by:

$$e_i = \alpha_i \Delta T + \beta_i \Delta c \tag{6}$$

Being α_i the coefficient of thermal expansion; ΔT the change in temperature; β_i the coefficient of moisture expansion; and Δc the change in moisture concentration.

$\left[\left(\pm 45/\pm 45\right)_s\right]_{as}$ anti-symmetric and $\left[\left(\pm 45/\pm 45\right)_s\right]_s$ symmetric laminates have been analyzed in this study.

A symmetric laminate, for each ply above the mid-plane, has a ply of the same thickness and material located at the same distance below the mid-plane and oriented in the same direction θ. Moreover, when plies have a single value of θ they are called regular angle-ply laminates [25].

The constitutive relation for a symmetric regular laminate is given by:

$$\begin{Bmatrix} \varepsilon_x^0 \\ \varepsilon_y^0 \\ \gamma_s^0 \\ \hdashline \kappa_x \\ \kappa_y \\ \kappa_s \end{Bmatrix} = \left[\begin{array}{ccc:ccc} a_{xx} & a_{xy} & 0 & 0 & 0 & 0 \\ a_{yx} & a_{yy} & 0 & 0 & 0 & 0 \\ 0 & 0 & a_{ss} & 0 & 0 & 0 \\ \hdashline 0 & 0 & 0 & d_{xx} & d_{xy} & d_{xs} \\ 0 & 0 & 0 & d_{yx} & d_{yy} & d_{ys} \\ 0 & 0 & 0 & d_{sx} & d_{sy} & d_{ss} \end{array}\right] \left(\begin{Bmatrix} N_x \\ N_y \\ N_s \\ \hdashline M_x \\ M_y \\ M_s \end{Bmatrix} + \begin{Bmatrix} N_x^{HT} \\ N_y^{HT} \\ 0 \\ \hdashline 0 \\ 0 \\ 0 \end{Bmatrix} \right) \tag{7}$$

The fact that the angle selected for the sequences studied in this work is 45º results in the following relations between compliance coefficients:

$$a_{xx} = a_{yy}; \quad d_{xx} = d_{yy}; \quad d_{xs} = d_{ys} \tag{8}$$

In addition, due to $\theta = 45^{\circ}$ the non-zero hygrothermal loads, N_x^{HT} and N_y^{HT} forces, are equal.

2.2.2. Out-of-plane relation

In this section the notation of Daniel and Ishai [26] has been used, being $yz = q$ and

$zx = r$. The constitutive relation corresponding to out-of plane shear strain components γ_q and γ_r is:

$$\begin{Bmatrix} \gamma_q \\ \gamma_r \end{Bmatrix}_k = \begin{bmatrix} S_{qq} & S_{qr} \\ S_{qr} & S_{rr} \end{bmatrix}_k \begin{Bmatrix} \tau_q \\ \tau_r \end{Bmatrix}_k \tag{9}$$

According to Eq.(2) γ_q and γ_r are independent from z and therefore Eq.(9) can be expressed in terms of average values of strain and stresses through the thickness:

$$\begin{Bmatrix} \overline{\gamma}_q \\ \overline{\gamma}_r \end{Bmatrix} = \frac{1}{h} \begin{bmatrix} \overline{S}_{qq} & \overline{S}_{qr} \\ \overline{S}_{qr} & \overline{S}_{rr} \end{bmatrix} \begin{Bmatrix} V_q \\ V_r \end{Bmatrix} \tag{10}$$

Where V_q and V_r are resultant shear forces per unit length and h denotes the thickness of the laminate. Equivalent compliance coefficients $\overline{S}_{ij}$ correspond to an average value of the whole laminate [27]. Given that in the present study all plies are oriented at $\theta = 45º$ and $\theta = -45º$, the absolute values of S_{ij} with $i, j = q, r$ are the same for both orientations.

2.3. Distribution of M_s and V_r

In the case that bending and twisting moments are present, the applicable equilibrium equation is [28]:

$$M_{x,x} + M_{s,y} - V_r = 0 \tag{11}$$

Considering that it is supposed that shear force V_r can be decomposed in a symmetric part related to bending V_r^b and an anti-symmetric part related to twisting V_r^t, Eq. (11) can be written in the following form:

$$\begin{aligned} M_{x,x} &= V_r^b \\ M_{s,y} &= V_r^t \end{aligned} \tag{12}$$

Since according to Eq.(2) $\gamma_q = 0$, from Eq. (10) it results that:

$$\overline{\gamma}_r = \frac{V_r}{h}\left(\overline{S}_{rr} - \frac{\overline{S}_{qr}^2}{\overline{S}_{qq}}\right) \tag{13}$$

According to Eq.(7), the twisting curvature can be expressed as:

$$\kappa_s = d_{xs} M_x + d_{ss} M_s \tag{14}$$

Considering that the bending moment M_x has been assumed to be uniform across the width, $M_{s,y}$ can be obtained differentiating Eq. (14) with respect to y:

$$M_{s,y} = d_{ss}^{-1} \kappa_{s,y} \tag{15}$$

Replacing Eq. (13) and Eq. (15) in Eq.(12), it results that:

$$d_{ss}^{-1} \kappa_{s,y} - h\overline{S}_{rr}^{-1} \overline{\gamma}_r^t = 0 \tag{16}$$

From Eq.(3) and Eq.(2), the twisting curvature and its derivative with respect to y result in:

$$\begin{aligned} \kappa_s &= \overline{\gamma}_{r,y} + 2\theta_y' \\ \kappa_{s,y} &= \overline{\gamma}_{r,yy} \end{aligned} \tag{17}$$

Replacing Eq.(17) in Eq.(16) and rearranging the expression:

$$\overline{\gamma}_{r,yy}^t - k^2 \overline{\gamma}_r^t = 0 \tag{18}$$

Where

$$k^2 = \frac{h d_{ss}}{\overline{S}_{rr} - \dfrac{\overline{S}_{qr}^2}{\overline{S}_{qq}}} \tag{19}$$

The general solution of Eq.(18) is:

$$\overline{\gamma}_r^t(y) = C_1 \sinh ky + C_2 \cosh ky \tag{20}$$

Differentiating Eq.(20) and replacing in Eq.(17) twisting curvature is obtained and can be replaced in Eq.(14) giving:

$$M_s = d_{ss}^{-1}\left[k\left(C_1 \cosh ky + C_2 \sinh ky\right) + 2\theta'_y - d_{xs}M_x\right] \tag{21}$$

Integration constants are obtained by imposing the boundary conditions $M_s = 0$ when $y = \pm\frac{1}{2}b$ to Eq.(21):

$$\begin{aligned} C_1 &= \frac{d_{xs}M_x - 2\theta'_y}{k\cosh\lambda} \\ C_2 &= 0 \end{aligned} \tag{22}$$

Where $\lambda = \frac{1}{2}kb$.

Replacing the constants in Eq.(21) the distribution of the twisting moment is determined:

$$M_s = \frac{d_{xs}M_x - 2\theta'_y}{d_{ss}}\left(\frac{\cosh ky}{\cosh\lambda} - 1\right) \tag{23}$$

Replacing the constants in Eq.(20) it results that:

$$\overline{\gamma}_r^t = \frac{d_{xs}M_x - 2\theta'_y}{k\cosh\lambda}\sinh ky \tag{24}$$

2.4. Complementary strain energy and its derivatives

Being $\left\{\overline{N}\right\}$ the matrix of the sum of mechanical and hygrothermal forces and $\left\{\overline{M}\right\}$ the matrix of the sum of mechanical and hygrothermal moments, the complementary strain energy in a multidirectional laminate due to in-plane stresses has been determined in [29], being:

$$U^* = \frac{1}{2}\int_{L_x}\int_{L_y}\left(\left\{\overline{N}\right\}^t[a]\left\{\overline{N}\right\} + 2\left\{\overline{N}\right\}^t[b]\left\{\overline{M}\right\} + \left\{\overline{M}\right\}^t[d]\left\{\overline{M}\right\}\right)dxdy - \frac{1}{2}LbB \tag{25}$$

Where

$$B = \sum_{k=1}^{n}\{e\}_k^t[Q]_k\{e\}_k\left(z_k - z_{k-1}\right) \tag{26}$$

z_k denotes the distance from the mid-plane to the lower surface of the k^{th} layer. L_x and

L_y indicate length and width direction respectively. L is the total length of the specimen. B has been extracted from the integral since it is a not L_x or L_y dependent term.

From the energy balance of a differential crack advance, assuming that U^* is an exact differential, the Engesser-Casitigliano theorem and the energy release rate *G* are derived [30]:

$$\delta_i = \left(\frac{\partial U^*}{\partial F_i} \right)_a \tag{27}$$

$$G = \frac{1}{b} \left(\frac{\partial U^*}{\partial a} \right)_{F_i} \tag{28}$$

Being F_i the generalized force; δ_i the generalized displacement in the direction of the generalized force; *b* the specimen width; and *a* the crack length.

Differentiating Eq.(25) with respect to F_i and a, taking into account that hygrothermal terms do not depend on those variables, Eq.(27) and Eq.(28) become in:

$$\delta_i = U^*_{,F_i} = b \int_{L_x} \begin{pmatrix} \{N\}^t_{,F_i} [a] \{\bar{N}\} + \{N\}^t_{,F_i} [b] \{\bar{M}\} \\ + \{M\}^t_{,F_i} [b] \{\bar{N}\} + \{M\}^t_{,F_i} [d] \{\bar{M}\} \end{pmatrix} dx \tag{29}$$

$$G = \frac{1}{b} U^*_{,a} = \frac{1}{b} \frac{\partial}{\partial a} \left[\frac{1}{2} \int_{L_x} \left(\{\bar{N}\}^t [a] \{\bar{N}\} + 2 \{\bar{N}\}^t [b] \{\bar{M}\} + \{\bar{M}\}^t [d] \{\bar{M}\} \right) dx \right] \tag{30}$$

As in Eq.(30) the integral limits depend on the crack length, Leibniz`s integral rule can be applied in order to obtain the derivative with respect to a. It states that given a function $f = f(x,a)$:

$$\frac{\partial}{\partial a} \int_{a(a)}^{b(a)} f(x,a)\, dx = \int_{a(a)}^{b(a)} \frac{\partial f(x,a)}{\partial a} dx + f\left[b(a), a\right] b`(a) - f\left[a(a), a\right] a`(a) \tag{31}$$

2.5. Bending moment

With the objective of determining the distribution of bending moments along the cracked arm, the approach presented in [7] has been followed. Fig. 3 shows a simplified model of the distributed forces ahead of the crack tip for the upper half of the DCB specimen based on the results of the elastic foundation models presented by different authors [16, 21]. The shape for the stress distribution presented by these models has been approached to the one caused by two triangular distributed forces q_1 and q_3. P is the applied load, a is the crack length, x_1, x_2 and x_3 are the lengths of the bases of the distributed loads, while q_{10} and q_{30} are their maximum intensities, located at sections 1 and 3 respectively.

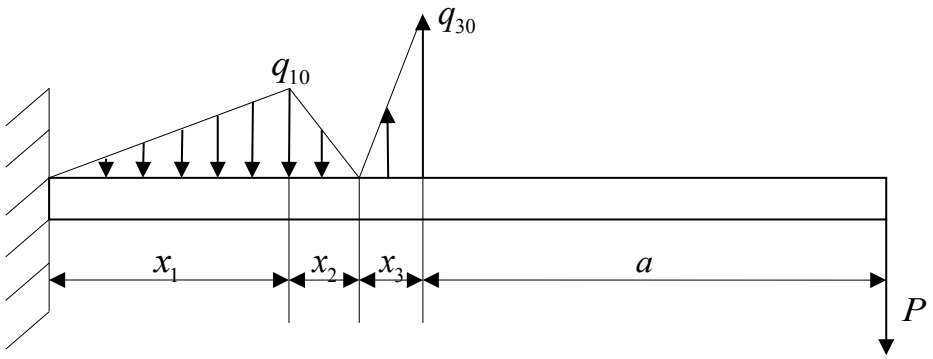

Fig. 3 Distributed force along the beam.

The distribution of bending moments is determined as a function of the bases and heights of the triangular distributed forces, which equilibrate the effect of the applied load. Thus, force and moment at the clamped end are null.

$$\begin{cases} m_{x_1} = -F_1 \dfrac{x^3}{3x_1^2} \\ m_{x_2} = \dfrac{F_1}{3x_2x_1}\left(x^3 - \left(3x_1 + 3x_2\right)x^2 + \left(3x_1^{\,2} + 3x_2x_1\right)x - x_1^{\,3} - x_2x_1^{\,2}\right) \\ m_{x_3} = -F_1\left(\dfrac{x_2 + x_1}{x_1}x + \dfrac{-x_2^{\,2} - 3x_2x_1 - 2x_1^{\,2}}{3x_1}\right) + F_3\dfrac{\left(x - x_1 - x_2\right)^3}{3x_3^{\,2}} \\ m_{x_a} = -F_1\left(\dfrac{x_2 + x_1}{x_1}x + \dfrac{-x_2^{\,2} - 3x_2x_1 - 2x_1^{\,2}}{3x_1}\right) + F_3\left(x - x_1 - x_2 - \dfrac{2x_3}{3}\right) \end{cases} \tag{32}$$

Where $F_1 = \frac{1}{2}q_{10}x_1$; $F_3 = \frac{1}{2}q_{30}x_3$.

Equating displacements at sections 1 to 3 to the ones corresponding to the transverse deformation and applying also static equilibrium, the values of x_1, x_2, x_3, q_{10} and q_{30} have been determined.

2.6. Symmetric laminate: redundant twisting moment

In the case of symmetric laminates, the fact that the rotation at the load application point is prevented combined with the difference in the sense of rotation shown in Figure 1, induces a reactive moment that is assumed to be concentrated at the crack front as it is shown in Fig. 4.

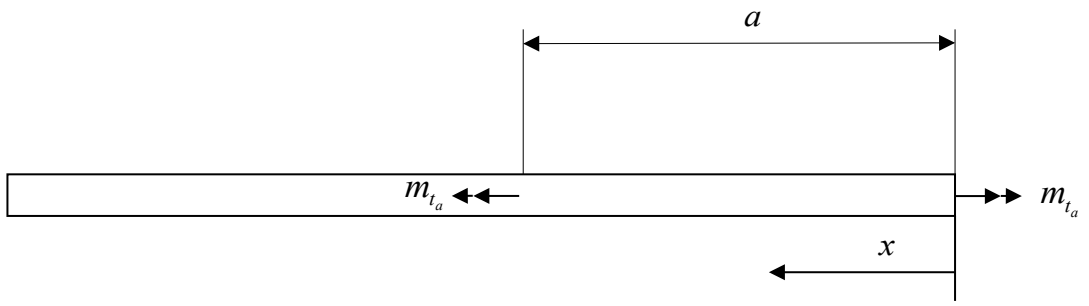

Fig. 4 Twisting moment in a cracked arm.

From Eq. (23) the distribution of the twisting moment per unit length is:

$$M_s = \frac{d_{xs} M_{x_a} - 2\theta'_y}{d_{ss}} \left(\frac{\cosh ky}{\cosh \lambda} - 1 \right) \tag{33}$$

Where M_{x_a} is the bending moment per unit length at the crack front. The half of the whole twisting moment m_t of a rectangular section corresponds to M_s and the other half correspond to the resultant moment of out-of-plane shear force V_r^t [31]:

$$m_t = \int_{L_y} M_s dy + \int_{L_y} V_r^t y dy \tag{34}$$

And thus:

$$m_t = 2\int_{L_y} M_s dy = \frac{2\left(d_{xs} M_{x_a} - 2\theta'_y\right)}{d_{ss}} b(\xi - 1) \tag{35}$$

Where:

$$\xi = \tfrac{1}{\lambda} \tanh \lambda \tag{36}$$

From Eq. (33) and Eq. (35) the relation between M_s and m_t is:

$$M_s = \frac{1}{2b(\xi - 1)} \left(\frac{\cosh ky}{\cosh \lambda} - 1 \right) m_t \tag{37}$$

Moment resultants are given by:

$$\left\{ \bar{M} \right\} = \begin{Bmatrix} M_x \\ 0 \\ M_s \end{Bmatrix} \tag{38}$$

The theorem of Engesser-Castigliano will be used in order to calculate the twisting moment applied by the piano hinges. Replacing Eq.(38) in Eq.(28) and taking into account the properties of symmetric laminates described in section 2.2.1, it gives:

$$U^*_{,m_{ta}} = \frac{1}{2} \int_{L_x} \int_{L_y} \left(2 d_{xs} M_x M_{s,m_{ta}} + 2 d_{ss} M_s M_{s,m_{ta}} \right) dx dy = 0 \tag{39}$$

Solving Eq.(39) the distribution of the twisting moment per unit length can be determined:

$$M_s = \frac{d_{xs}}{d_{ss}} \frac{(\xi - 1)}{3(1-\xi) - \lambda^2 \xi^2} \left(\frac{\cosh ky}{\cosh \lambda} - 1 \right) \frac{Pa}{b} \tag{40}$$

Replacing the distribution given in Eq. (40) in Eq. (37) twisting moment applied the piano hinges is:

$$m_{t_a} = \frac{d_{xs}}{d_{ss}} \frac{2(\xi - 1)^2}{3(1-\xi) - \lambda^2 \xi^2} Pa \tag{41}$$

Fig. 5 shows the distribution through the width of the normalized twisting moment with respect to the applied load, for the material and stacking sequence used for testing in this study, when $a = 50mm$.

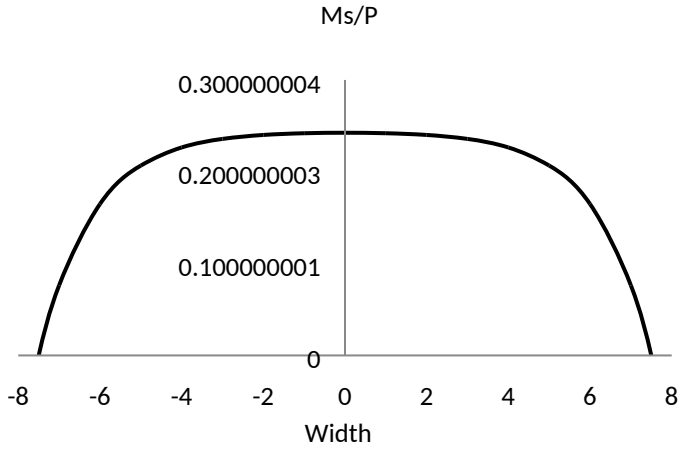

Fig. 5 Distribution of the twisting moment through the width.

2.7. Antisymmetric laminate: Shear force

In the case of an anti-symmetric DCB specimen, in absence of load, cracked arms remain horizontal from the load application point to the crack front. In the non-cracked part of the laminate hygrothermal twisting moment generates rotations, but that effect is considered negligible with respect to those related to bending-twisting coupling in the cracked arms. When load begin to increase the coupling generates a rotation of the same sense in both cracked arms. Taking into account that the specimen remains horizontal at

the load application point, the crack front has to rotate an angle θ_y as can be seen in Fig. 6. Therefore, there are opposite in plane N_s forces in each cracked arm related to mode III fracture.

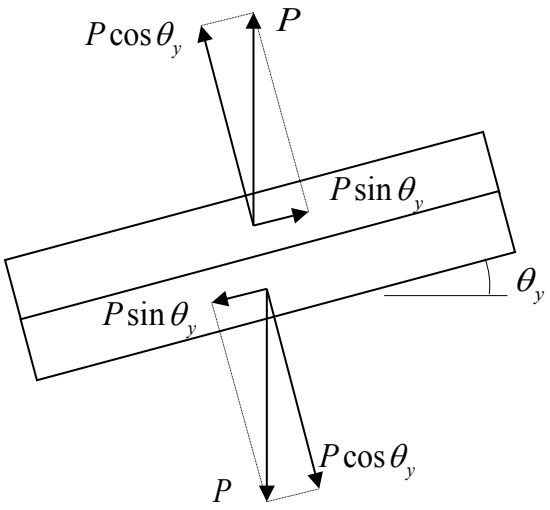

Fig. 6 P force and its components at the crack tip.

Force and moment resultants for this case are:

$$\left\{\bar{N}\right\}=\begin{Bmatrix} N_x^{HT} \\ N_y^{HT} \\ N_s \end{Bmatrix} \tag{42}$$

$$\left\{\bar{M}\right\}=\begin{Bmatrix} M_x \\ 0 \\ 0 \end{Bmatrix} \tag{43}$$

The twisting angle per unit length rotated by the cracked arms can be obtained from Eq.(23):

$$2\theta_y^{'}=d_{xs}M_x-\frac{d_{ss}M_s}{\dfrac{\cosh ky}{\cosh\lambda}-1} \tag{44}$$

Taking into account that $M_s=0$ and $M_x=\dfrac{1}{b}Px$ in the cracked section, after integrating

Eq.(44):

$$\theta_y = \frac{d_{xs}}{4b} P x^2 \tag{45}$$

Assuming that the angle is very small, $\sin\theta_y \approx \theta_y$ and thus the distribution of shear force per unit length can be expressed as:

$$N_s = \frac{d_{xs}}{4b^2} P^2 x^2 \quad 0 < x < a \tag{46}$$

2.8. Energy Release Rate

2.8.1. Symmetric laminate $\left[\left(\pm 45/\pm 45\right)_s\right]_s$

With the aim of obtaining an expression of the energy release rate as a function of the crack length, the compliance coefficients and applied loads, given in Eq.(7) and Eq.(38) respectively, are replaced in Eq.(30).

$$\begin{aligned} G = {} & \frac{2}{b}\int_{L_x}\int_{L_y}\left(d_{xx}M_x M_{x,a} + d_{xs}M_s M_{x,a} + d_{xs}M_x M_{s,a} + d_{ss}M_s M_{s,a}\right)dxdy \\ & + \frac{1}{b}\int_{L_y} d_{ss}M_s^2 dy \end{aligned} \tag{47}$$

The term affected by d_{xx} is directly related to the applied bending moment and thus the predominant part of the energy release rate due to fracture mode I. The terms affected by d_{xs} are related to bending-twisting coupling. The terms affected by d_{ss} are related to twisting. It is worth noting that the last term corresponds to Leibniz`s integral rule.

Taking into account those considerations, replacing the expressions for bending moments and twisting moments obtained in Eq.(32) and Eq.(40) in Eq.(47), it results:

$$G_I(bending) = \frac{P^2 d_{xx}}{b^2}\left(\alpha_0 + \alpha_1 a + a^2\right) - \frac{d_{xs}^2}{d_{ss}}\frac{\left(\xi - 1\right)^2}{3(1-\xi) - \lambda^2\xi^2}\left(\frac{Pa}{b}\right)^2 \tag{48}$$

$$G_I(twisting) = -\frac{1}{2}\frac{d_{xs}^2}{d_{ss}}\frac{(\xi-1)^2}{3(1-\xi)-\lambda^2\xi^2}\left(\frac{Pa}{b}\right)^2 \tag{49}$$

Where factors α_0 and α_1 are factors that depend on the dimensions x_1, x_2 and x_3.

The negative sign is because the twisting moment facilitates the crack growth. It is worth noting that the effect of the twisting moment is a non-uniform aperture across the width, as shown in Fig. 1. That fracture mode corresponds to mode I and no to mode III as we erroneously stated in the case of hygrothermal effects in ref. [24].

2.8.2. Anti-symmetric laminate $\left[\left(\pm 45/\pm 45\right)_s\right]_{as}$

Similarly to section 2.8.1, compliance matrices in Eq. (7) and applied loads in Eq. (42) and Eq. (43) can be replaced in Eq.(30):

$$G = \frac{2}{b}\int_{L_x}\int_{L_y}\left(d_{xx}M_x M_{x,a} + a_{ss}N_s N_{s,a}\right)dxdy + \frac{1}{b}\int_{L_y} a_{ss}N_{s_a}^2 dy \tag{50}$$

In this case, since there is not in-plane-out-of-plane couplings, contributions to different modes are separated. While the first term, affected by d_{xx}, is related to mode I, the others terms, preceded by a_{ss} coefficient correspond to fracture mode III.

Replacing bending moments and forces obtained in (32) and (46) in Eq.(50):

$$G_I = \frac{d_{xx}P^2}{b^2}\left(\alpha_0 + \alpha_1 a + a^2\right) \tag{51}$$

$$G_{III} = \frac{a_{ss}d_{xs}^2P^4}{16b^2}a^4 \tag{52}$$

2.9. Displacement of the load application point

With the aim of obtaining the values of crack length used to calculate G, the method presented in [7] will be used. This method leads to calculate an effective crack length for every pair of load and displacement values based on the change of the compliance. The procedure consists on equating the compliance experimentally obtained with the one analytically determined. As the method has been described for unidirectional specimens, additional terms related to bending-twisting coupling should be added. These terms are consequence of the bending curvatures generated by twisting moments and therefore, are applicable in the case of symmetric specimens. In the case of anti-symmetric laminates, twisting curvatures generated by bending moments do not change the vertical displacement of the specimen centre.

Replacing the compliance matrices and applied loads, given in Eq.(7) and Eq.(38), in Eq.(29):

$$\delta = \int_{L_x}\int_{L_y}\left(d_{xx}M_x M_{x,P} + d_{xs}M_s M_{x,P} + d_{xs}M_x M_{s,P} + d_{ss}M_s M_{s,P}\right)dxdy \tag{53}$$

Solving the integral with the expressions for bending and twisting moments above determined, Eq.(53) leads to:

$$\delta = d_{xx}\frac{P}{b}\left(\frac{1}{3}a^3 + \frac{\alpha_1}{2}a^2 + \alpha_0 a + \alpha\right) - \frac{1}{2}\frac{d_{xs}^2}{d_{ss}}\frac{(\xi-1)^2}{3(1-\xi)-\lambda^2\xi^2}\frac{P}{b}a^3 \tag{54}$$

Where α, as factors α_0 and α_1, depends on the dimensions x_1, x_2 and x_3.

3. Experimental

3.1. Material and apparatus

Elementary plies of T6T/F593, a thermosetting epoxy resin (F593) reinforced by Toray T300 continuous carbon fiber provided by Hexcel Composites with a 55% volume-

content of fiber, were used to produce laminates. Two kinds of sixteen-layered angle-ply laminates with a Teflon film embedded in the center plane during the piling up process in order to make the initial crack were manufactured by hot press molding. Specimens were cut with a diamond disc saw, being the nominal thickness and width 3 mm and 15 mm respectively. The edges of the laminate were discarded for the preparation of the specimens. Piano hinges were bonded to the specimens and tests were performed using a universal testing machine MTS–Insight 10 with a load cell of 250 N. The mechanical and thermal characteristics of unidirectional prepregs are summarized in **Table 1**.

$E_x(GPa)$	$E_y(GPa)$	$G_{xy}(GPa)$	ν_{xy}	$\alpha_1(^oC^{-1})$	$\alpha_2(^oC^{-1})$
124	8.4	4.7	0.3	$-4.5\cdot10^{-9}$	$5.2\cdot10^{-5}$

Table 1 Mechanical and thermal properties of the unidirectional ply

3.2. Preliminary tests

With the aim of determining the elastic properties E_f and G_{13}, the procedure based on three-point bending tests at different spans proposed by Mujika [32] was used, obtaining similar results for both stacking sequences. The average longitudinal flexural modulus is $14.2GPa$ and the shear modulus $4GPa$.

Specimen displacement (δ_{spec}) was determined from load–displacement curves. The experimental displacement ($\delta_{\exp}$) is the addition of the specimen displacement and the displacement due to the system compliance (C_s).

$$\delta_{espec} = \delta_{\exp} - C_s P \tag{55}$$

The system compliance was determined testing a thin steel plate with bonded piano hinges as a DCB specimen. Being the deformation of the plate negligible, the slope of

the obtained load–displacement curves can be considered to be the effect of the system compliance. The average value obtained for the stiffness of the system is $C_s = 201 \cdot 10^{-5}\, mm / N$.

4. Results

4.1. Test considerations

In order to compare results obtained through the presented method with those obtained by means of the "area" method and the modified beam theory (MBT) with crack length correction proposed by Williams [16]. The last one has been used by several authors for calculating G_I in multidirectional laminates [33, 34, 35], and according to Shokrieh [36] it leads to reliable results in angle-ply DCB specimens. These methods have been selected meaning to avoid using propagation values. In the case of the "area method", since it requires a propagation data, a minimum growth of 1 mm has been considered.

The deviation from linearity point has been used to determine the crack onset value for the calculations presented in this study

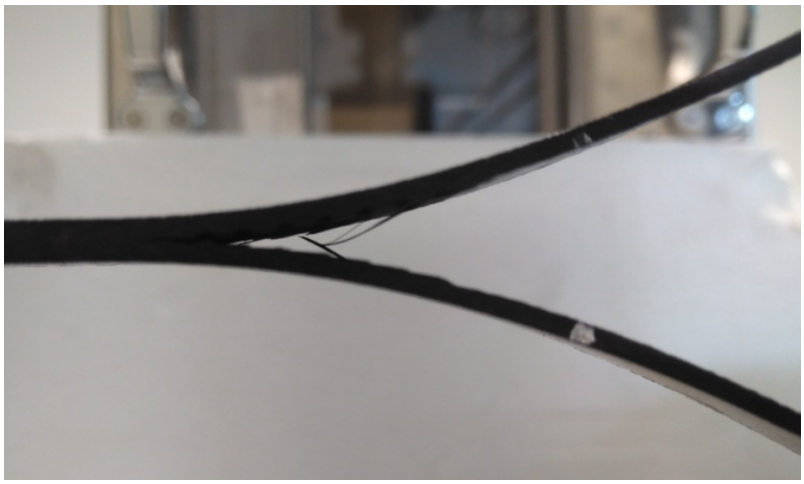

Fig. 7 DCB test. Crack propagation phase.

Several specimens of both sequences have been tested with the aim of determining the Energy Release rate. The initial crack length varies between 40mm and 60mm. As can be observed in Fig. 7, the crack advanced simultaneously in the mid-layer and in the adjacent ply in a zig-zag fashion, without translaminar advances as in [24]. Therefore, in this case, specimens have remained horizontal during the propagation phase. This leads to the geometrical structure shown in **Error! Reference source not found.**, that is similar to the one observed in cross-ply specimens [37].

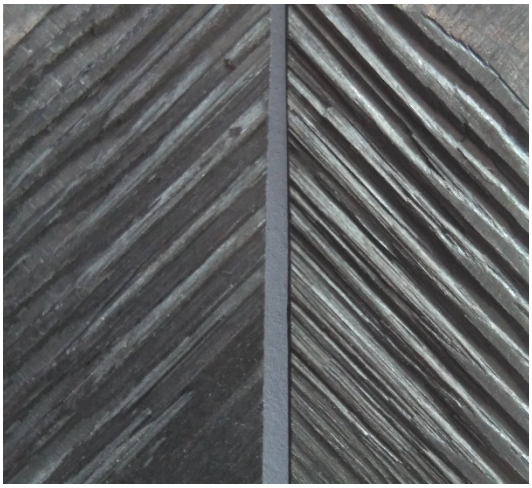

Fig. 8 Crack propagation surfaces

4.2. Critical Energy Release Rate

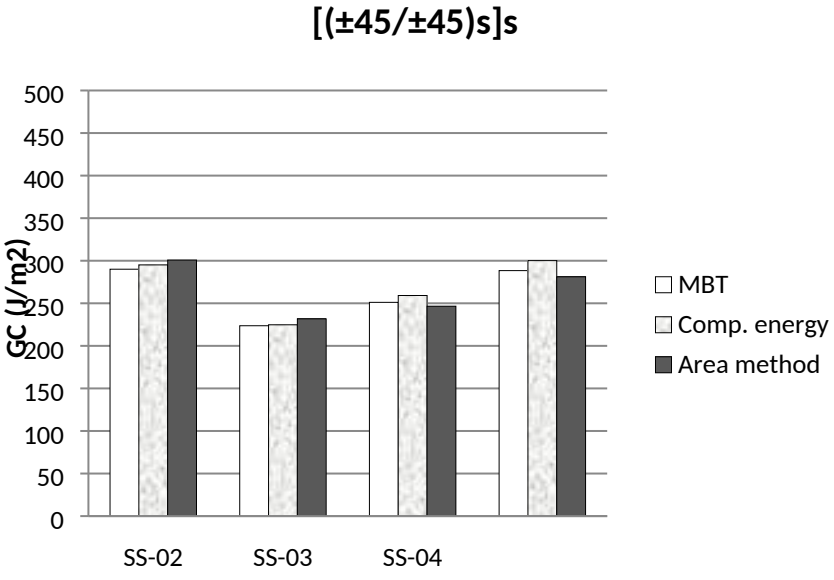

Fig. 9 Critical energy release rate for four symmetric specimens.

Considering the propagation behavior observed only initiation values will be considered to calculate interlaminar properties. Fig. 9 shows the comparison of the G_c values obtained for four symmetric specimens. As can be observed, although results for different specimens vary significantly, the values for each specimen through the three methods used are similar. The maximum value of the bending-twisting effect for the specimens tested has been $G_I(coupling) = -2.3J/m^2$. It is worth noting that this value includes the terms affected by d_{xs} in Eq.(48) and Eq.(49).

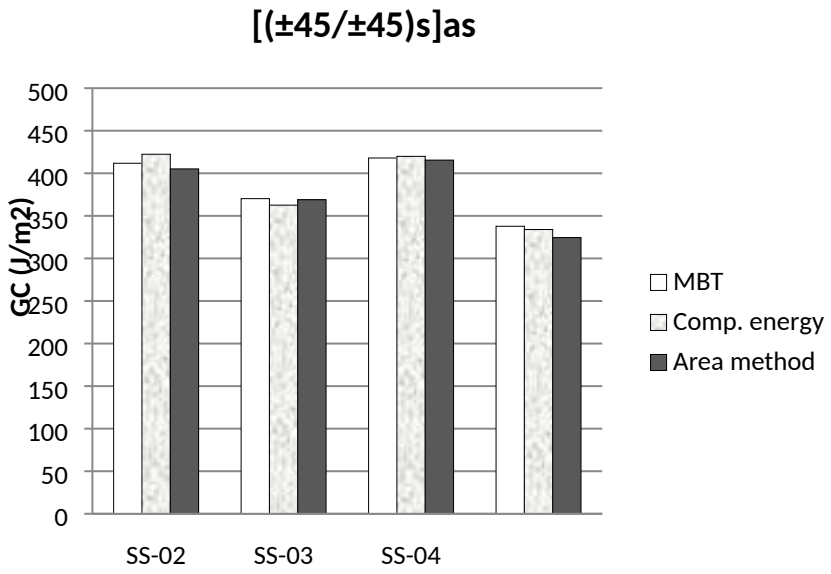

Fig. 10 Critical energy release rate for four anti-symmetric specimens.

Results obtained for anti-symmetric laminates are shown in Fig. 10, and as in the case of symmetric laminates, values for different specimens also vary quite a lot while values obtained for each specimen through different methods are very similar. For this configuration, the negative term that includes the rotation in the crack tip results in a maximum of $G_{III} = -1,2 \cdot 10^{-6} J/m^2$.

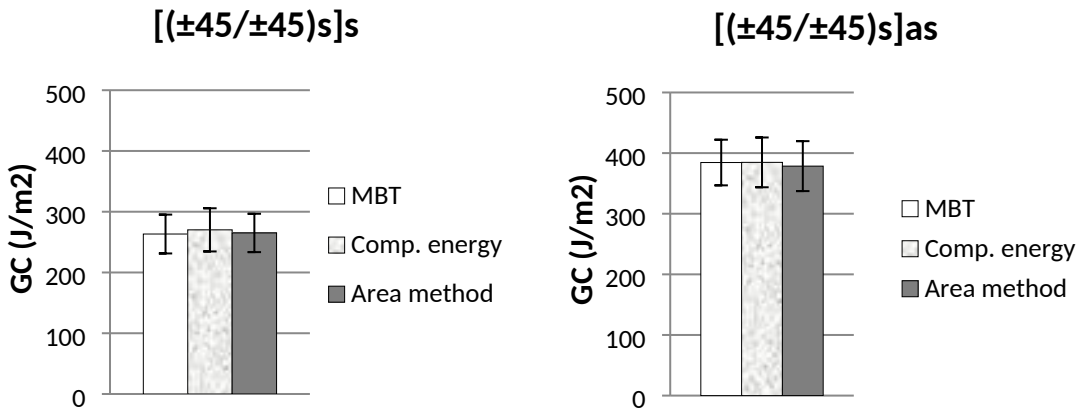

Fig. 11 Average critical Strain Energy Release Rate. a) Symmetric laminate. b) Anti-symmetric laminate.

Fig. 11 shows the average values for G_C calculated for both configurations studied. The mean value and the standard deviation obtained by the complementary energy are:

Symmetric laminate: $G_c = 270 \pm 35\, J/m^2$

Anti-symmetric laminate: $G_c = 385 \pm 44\, J/m^2$

The lower value in the symmetric laminate is attributed to the additional aperture in mode I related to the bending-twisting coupling. Indeed, the normal stresses distribution in the interface is not uniform. This fact has been taken into account replacing that non-uniformity by the resultant and the resultant twisting moment through the width. Nevertheless, normal stress values are higher in the open side of Fig. 1 in the symmetric case. The fact that both plies in the middle surface, where crack advances, have the same orientation could be an additional factor related to lower values of G_c in the symmetric case.

5. Summary and conclusions

Symmetric and anti-symmetric angle-ply DCB specimens with symmetric cracked arms

have been studied. The analysis presented leads to obtain an expression for determining the energy release rate in both cases.

A non-uniform distribution of the twisting moment per unit length across the width has been considered in the study, leading to determine the effect of the bending-twisting coupling. In the case of symmetric laminates, the fact that rotation at the load application point is prevented combined with the opposite sense of rotation of each arm, induces a reactive moment at the crack front. In the case of anti-symmetric laminates, as the sense of rotation is the same in both arms, the crack front rotates with respect to the load application point.

In the analysis of symmetric specimens, the effect of the bending curvatures generated by twisting moments on the displacement at the load application point has been determined. The expressions obtained have been compared experimentally with two methods: the area method and the corrected beam theory with crack correction. The results obtained are similar for the three methods. These results show that the value of the energy release rate is higher when testing anti-symmetric laminates. It has been attributed to the non-uniform aperture in the crack tip due to the bending-twisting coupling and to the different orientation of the plies adjacent to the center plane.

6. Funding

Financial support of the University of the Basque Country (UPV/EHU) under program GIU 16/51 is acknowledged.

References

[1] T. Anderson, Fracture Mechanics-Fundamentals and Applications 3rd edn., Taylor & Francis Group, 2005.
[2] ISO, « 15024, Fiber-reinforced Plastic Composites – Determination of Mode I Interlaminar Fracture Toughness, GIc, for Unidirectionally Reinforced Materials,» (2001.
[3] ASTM, «Standard D5528-94a, Standard Test Method for Mode I Interlaminar Fracture Toughness of Unidirectional Continuous Fiber Reinforced Polymer Matrix Composites,» Philadelphia, 1994.
[4] A. Szekrényes, «Prestressed fracture specimen for delamination testing of composites,» *International Journal of Fracture,* nº 139, pp. 213-237, 2006.
[5] H. Yoshihara y T. Kawamura, «Mode I fracture toughness estimation of wood by DCB test,» *Composites: Part A,* vol. 37, p. 2105–2113, 2006.
[6] M. F. S. F. De Moura, J. J. L. Morais y N. Dourado, «A new data reduction scheme for mode I wood fracture characterization using the double cantilever beam test,» *Engeneering fracture mechanics,* vol. 75, pp. 3852-3865, 2008.
[7] J. De Gracia, A. Boyano, A. Arrese y F. Mujika, «A new approach for determining the R-curve in DCB tests without optical measurements,» *Engineering Fracture Mechanics,* vol. 135, pp. 274-285, 2015.
[8] M. J. Hiley, «Delamination between multi-directional ply interfaces in carbon-epoxy composites under static and fatigue loading,» *European Structural Integrity Society,* vol. 27, pp. 61-72, 2000.
[9] A. B. De Morais, M. F. de Moura, A. T. Marques y P. T. de Castro, «Mode-I interlaminar fracture of carbon/epoxy cross-ply composites,» *Composites Science and Technology,* vol. 62, p. 679–686, 2002.
[10] A. B. Pereira y A. B. de Morais, «Mode I interlaminar fracture of carbon/epoxy multidirectional laminates,» *Composites Science & Technology,* vol. 64, pp. 2261-2270, 2004.
[11] N. S. Choi, A. J. Kinloch y J. G. Williams, «Delamination Fracture of Multidirectional Carbon-Fiber/Epoxy Composites under Mode I, Mode II and Mixed Mode I/II Loading,» *Journal of Composite Materials,* vol. 33, nº 1, pp. 73-100, 1999.
[12] A. B. De Morais, «Double cantilever beam testing of multidirectional laminates,» *Composites: Part A,* vol. 34, nº 12, p. 1135–1142, 2003.
[13] M. M. Shokrieh, M. Heidari-Rarani y M. R. Ayatollahi, «Calculation of GI for a multidirectional composite double cantilever beam on two-parametric elastic foundation,» *Areospace Science and Technology,* vol. 15, pp. 534-543, 2011.
[14] A. B. De Morais, «Double cantilever beam testing of multidirectional laminates,» *Composites: Part A,* vol. 34, nº 12, pp. 1135-1142, 2003.
[15] M. F. Kanninen, «An augmented double cantilever beam model for studying crack propagation and arrest,» *International Journal of Fracture,* vol. 9, nº 1, p. 83.92, 1971.
[16] J. G. Williams, «End corrections for orthotropic DCB specimens,» *Compos Sci Technol,* vol. 35, nº 4, pp. 367-376, 1989.
[17] F. Ozdil y L. Carlsson, «Beam analysis of angle-ply laminate DCB specimens,» *Composites Science and Technology,* vol. 59, pp. 305-315, 1999.
[18] A. Szekrényes, «Improved analysis of unidirectional composite delamination specimens,» *Mechanics of Materials,* vol. 39, pp. 953-974, 2007.
[19] R. Olsson, «On improper foundation models for the DCB,» de *16th International Conference on Composite Materials*, 2007.
[20] J. M. Whitney, «Stress analysis of the double cantilever beam specimen,» *Compos Sci Technol,* vol. 23, p. 201–219, 1985.
[21] K. Kondo, «Analysis of double cantilever beam specimen,» *Advanced Composite Materials,* vol. 4, nº 4, pp. 355-366, 1995.
[22] J. R. Weatherby, *Evaluation of energy release rates in unidirectional double cantilevered beam fracture specimens,* MSc Thesis: Texas A&M University, 1982.
[23] V. A. Franklin y T. Christopher, «Fracture Energy Estimation of DCB Specimens Made of GlassEpoxy, An Experimental Study,» *Advances in Materials Science and Engineering,* vol. 2013, p. 7, 2013.
[24] J. De Gracia, A. Boyano, A. Arrese y F. Mujika, «Analysis of the DCB test of angle-ply laminates including residual stresses,» *Theoretical and Applied Fracture Mechanics,* In press.
[25] I. Daniel y O. Ishai, Engineering mechanics of composite materials, New York: Oxford university press , 2006.
[26] I. M. Daniel y O. Ishai, Engineering Mechanics of Composite Materials, New York: Oxford

University Press, 1994.
[27] J. Romera, M. Cantera, I. Adarraga y F. Mujika, «A top-down analytic approach for the analysis of edge effects of angle-ply symmetric laminates,» *Composite Structures,* vol. 104, pp. 60-70, 2013.
[28] J.-M. Berthelot, Matériaux composites. 5th ed., Paris: Tec&>Doc Lavoisier, 2012.
[29] F. Mujika, «A novel approach for the three point flexure test of multidirectional laminates,» *Journal of Composite Materials,* vol. 46, nº 3, pp. 259-274, 2011.
[30] A. Boyano, J. de Gracia, A. Arrese y F. Mujika, «Equivalent energy release rate and crack stability in the End Notched Flexure with inserted roller mixed mode I/II test,» *Theoretical and Applied Fracture Mechanics,* vol. 87, pp. 99-109, 2017.
[31] V. Vasiliev y E. Morozov, Advanced mechanics of composite materials, Elsevier Science and Technology, 2007.
[32] F. Mujika, «On the effect of shear and local deformation in three-point bending tests,» *Polym Test,* vol. 26, pp. 869-877, 2007.
[33] A. Laksimi, A. Ahmed Benyahia, M. L. Benzeggagh y X. L. Gong, «Initiation and bifurcation mechanisms of cracks in multi-directional laminates,» *Composites Science and Technology,* vol. 60, pp. 597-604, 2000.
[34] A. De Morais, «A new fibre bridging based analysis of the Double Cantilever Beam (DCB) test,» *Composites: Part A,* vol. 42, p. 1361–1368, 2011.
[35] P. Qiao y F. Chen, «On the Compliance and Energy Release Rate of Generically-unified Beam-type Fracture Specimens,» *Journal of Composite Materials,* vol. 45, pp. 65-101, 2011.
[36] M. M. Shokrieh y M. Heidari-Rarani, «A comparative study for beams on elastic foundation models to analysis of mode-I delaminations in DCB specimens,» *Structural Engineering and Mechanics,* vol. 37, nº 2, pp. 149-162, 2011.
[37] A. B. De Morais, M. F. de Moura, A. T. Marques y P. T. de Castro, «Mode-I interlaminar fracture of carbon/epoxy cross-ply composites,» *Composites Science and Technology,* vol. 62, pp. 679-686, 2002.
[38] B. Davidson, R. Krüger y M. König, «Effect of stacking sequence on energy release rate distributions in multidirectional dcb and enf specimens,» *Engineering Fracture Mechanics,* vol. 55, nº 4, pp. 557-569, 1996.
[39] X. J. Gong, A. Hurez y G. Verchery, «On the determination of delamination toughness by using multidirectional DCB specimens,» *Polymer Testing,* vol. 29, pp. 658-666, 2010.
[40] S. Hashemi, A. J. Kinloch y J. G. Williams, «Corrections needed in double-cantilever beam tests for assessing the interlaminar failure of fibre-composites,» *Journal of Materials Science Letters,* vol. 8, pp. 125-129, 1989.